Journal of Materials Processing Tech. 264 (2019) 336–345

Contents lists available at ScienceDirect

Journal of Materials Processing Tech.

journal homepage: www.elsevier.com/locate/jmatprotec

An approach to enhancement of Mg alloy joint performance by additional pass of friction stir processing

Q. Shang[a,b], D.R. Ni[a,*], P. Xue[a], B.L. Xiao[a], K.S. Wang[c], Z.Y. Ma[a,c,*]

[a] Shenyang National Laboratory for Materials Science, Institute of Metal Research, Chinese Academy of Sciences, 72 Wenhua Road, Shenyang, 110016, China
[b] School of Materials Science and Engineering, University of Science and Technology of China, 72 Wenhua Road, Shenyang, 110016, China
[c] School of Metallurgical Engineering, Xi'an University of Architecture and Technology, Xi'an, 710055, China

ARTICLE INFO

Associate Editor: C. H. Cateres

Keywords:
Mg alloy
Friction stir processing
Joint performance enhancement
Texture
Twinning

ABSTRACT

Profuse extension twins were successfully introduced to the whole stir zone of friction stir welded AZ31 alloy, and the joint turned out to be a two-layered structure after an additional pass of friction stir processing with a different tool under appropriate parameters. The detailed twinning characteristics and resultant texture evolution in various regions were then investigated. The strengthening effect of twin lamellae and the weakened strain localization in deformation gave rise to a significant improvement of joint mechanical properties. The yield strength of the joint was raised from 96 MPa to 122 MPa and the tensile strength was enhanced to be roughly equal to that of the base material with no reduction of elongation.

1. Introduction

Unlike fusion welding, which is susceptible to defects such as porosity, oxidation, and high residual stress when joining Mg alloys, friction stir welding (FSW), as a solid state joining technique, has been extensively used to obtain sound welds with uniform equiaxed fine grains (Mishra and Ma, 2005).

Despite the optimized microstructure and fewer defects, degradation of mechanical performance after FSW has still been frequently reported in various kinds of wrought Mg alloys, such as rolled AZ31 (Commin et al., 2009), extruded AZ31 (Shang et al., 2017a), extruded AZ80 (Yang et al., 2014), extruded ZK60 (Xie et al., 2008) and so on. Many prior studies have suggested that the reduction of tensile properties is mainly associated with the special strong texture evolved in FSW joints. Park et al. (2003a,b) found that typical texture distribution usually forms in the stir zone (SZ) with the basal planes of grains roughly situated around the pin surface, and the tensile properties of weld are strongly influenced by this crystallographic orientation distribution. Woo et al. (2006) also demonstrated the drastic texture changes across the SZ boundaries by neutron-diffraction measurements, and found that the incompatible SZ boundaries could cause a fracture in tensile deformation. Shang et al. (2017a) suggested the difference of local crystallographic orientation in the SZ between the advancing side (AS) and the retreating side (RS), which significantly influenced the fracture location and propagation. Ascribed to the specifically-distributed microtexture, severe strain localization was usually found inevitable in the loaded joints. To elucidate the texture effect on the strain distribution behavior, Liu et al. (2014) evaluated the different involvement of slip and twinning in different sub-regions of the SZ by calculating the Schmid factor based on the texture distribution, and revealed that the preferentially activation of both basal slip and extension twinning near SZ boundaries led to the degradation of strength and especially yield strength. Shang et al. (2017b) analyzed the texture evolution in different sub-regions during the whole tensile deformation process. The continuous lattice rotation in SZ gave rise to the gradually softened orientation and accelerated strain localization near SZ boundaries. To obtain intuitive verification of the relationship between the microtexture and strain distribution, Mironov et al. (2017) detected the actual strain distribution by digital image correlation, and demonstrated the strain concentration in the locations with favorable orientation for basal slip. In the transverse tensile deformation of joints, the sub-region near the SZ-boundary on the AS was frequently reported as a soft-oriented area susceptible to significant deformation concentration and thus cracks. There is no doubt that this texture-induced strain localization can bring about premature failure and deteriorate the joint performance, which is detrimental to the structural application of FSW Mg alloys.

Researchers have tested successive processing techniques, aiming to enhance the mechanical properties of FSW Mg alloys, and found that texture modification by subsequent deformation could be an effective

* Corresponding authors at: Shenyang National Laboratory for Materials Science, Institute of Metal Research, Chinese Academy of Sciences, 72 Wenhua Road, Shenyang, 110016, China.
E-mail addresses: drni@imr.ac.cn (D.R. Ni), zyma@imr.ac.cn (Z.Y. Ma).

https://doi.org/10.1016/j.jmatprotec.2018.09.021
Received 22 April 2018; Received in revised form 16 September 2018; Accepted 17 September 2018
Available online 22 September 2018
0924-0136/

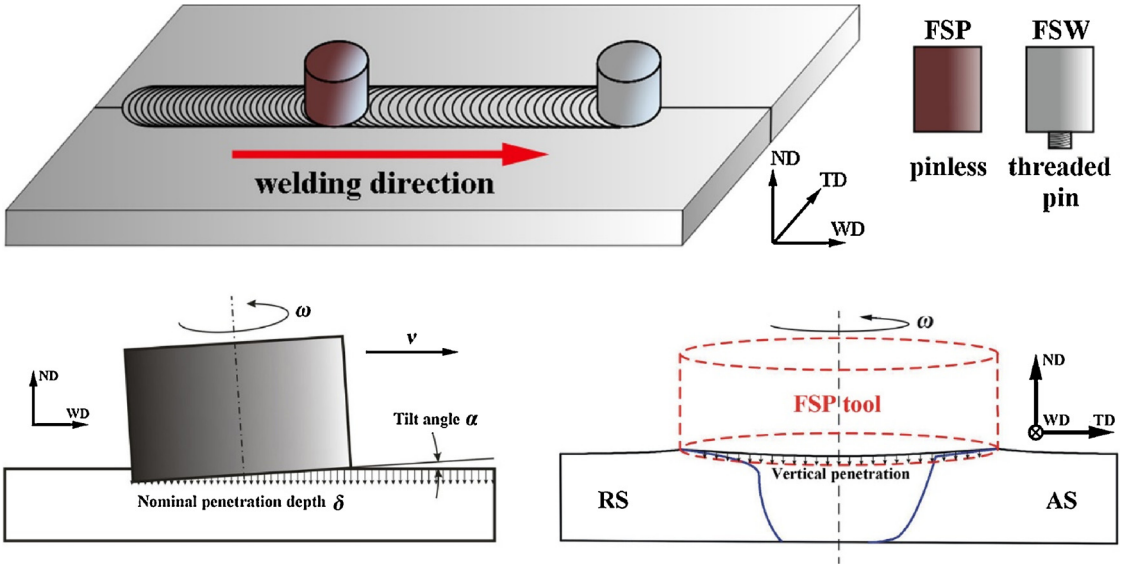

Fig. 1. Schematic illustration of the additional FSP method.

Table 1
Processing variable combinations of the additional FSP parameters.

	Tool rotation rate ω, rpm	Advancing speed ν, mm/min	Nominal penetration depth δ, mm
FSP-1	200	50	0.4
FSP-2	200	50	0.8
FSP-3	200	50	1.2
FSP-4	100	50	0.8
FSP-5	50	50	1.2

approach. Lee et al. (2007) conducted a subsequent compression along the normal direction (ND) of friction stirred AZ61 and achieved a significant improvement of yield strength. Xin et al. (2013, 2014a) explored various processing routes, such as post-rolling and subsequent tension along the transverse direction (TD) combined with annealing. Liu et al. (2016) even imposed subsequent compression along the welding direction (WD). They all successfully achieved enhancement of joint performance with these methods.

These processing methods are not practical in the actual manufacturing of complex structural components, as large-scale deformation processes are not usually expected to be used after welding. Subsequent rolling or compression along the ND is difficult and only applicable to welding sheet materials. Subsequent tension along the TD or compression along the WD is typically infeasible in operation. These processing methods would inevitably introduce large deformation and size changes to the whole component, which also limits their practical application.

A feasible and convenient method was required to enhance the joint performance of FSW Mg alloys. Based on the concept of FSW, a series of derived techniques have emerged for further application, as reviewed by Padhy et al. (2018). Friction stir processing (FSP), for instance, is proved effective and flexible by Raja and Pancholi (2017) for microstructure modification on a limited processing scale. With the aim to process the weld region only, an approach to joint optimization was developed by simply conducting an additional pass of FSP with a second rotational tool along the original FSW weld. Only the rotational tool needs replacing—there is no demand for any new or large-scale processing equipment for this post-weld processing. A series of FSP parameters were examined to seek an optimum processing method. Detailed investigations on the microstructure and texture evolution were conducted to unravel the joint-strengthening mechanism of this process.

2. Experimental

Commercial AZ31 alloy (Mg-3.3 wt.% Al-0.9 wt.% Zn) extruded plates with a thickness of 6.4 mm were used as a base material (BM). Sound FSW welds were created transverse to the plate extrusion direction using a tool composed of a concave shoulder and a cylindrical pin with thread features. The shoulder diameter is 24 mm; the pin is 5.8 mm in length and 8 mm in diameter. In the welding process, the tool was tilted at an angle of 2.5° and rotated at a rate of 800 rpm. The tool advancing speed was 100 mm/min. After FSW, an additional pass of FSP was conducted using a pinless tool with a flat shoulder (with equal diameter to that of FSW tool) at the same tool tilt angle, along the original weld with no location displacement, as illustrated in Fig. 1. A series of different combinations of critical variables like tool rotational rate ω, advancing speed ν, and nominal penetration depth δ (i.e., the programmed tool's vertical downward displacement before FSP) were adopted with an attempt to seek an optimized processing route, shown in Table. 1.

To characterize the microstructure at different length scales, optical microscopy (OM) and transmission electron microscopy (TEM) were adopted. The electron backscattered diffraction (EBSD) was used to analyze the texture evolution. The samples for these characterization methods were all cut perpendicular to the WD. The OM samples were mechanically polished and then etched with a solution of 10 mL glacial acetic acid + 10 mL distilled water + 70 mL ethanol + 4.2 g picric acid. The EBSD samples were prepared by electro-polishing using a solution of 90 mL ethanol + 10 mL perchloric acid and examined by an EBSD detector equipped in a Supra 55 scanning electron microscope (SEM). The TEM observations were performed using an FEI Tecnai G^2 20 transmission electron microscope.

To verify the effect of the additional FSP on the joint mechanical performance, transverse tensile properties of BM, FSW and FSP joints were examined at a same strain rate of 1×10^{-3} s^{-1}. All tensile specimens (with a gauge section of 40 mm in length and 10 mm in width) were cut by electrical discharge machining with the tensile direction perpendicular to WD, and then surface-ground. Tensile test of BM, original FSW joints and the FSP joints with the best mechanical performance was repeated three times. To directly elucidate how the additional FSP modifies the actual strain localization in the tensile deformation of joints, therefore improving the joint performance, comparative examinations of strain distribution by digital image correlation (DIC) were conducted on both the original FSW joints and the FSPed joints. The hardness profiles were measured across the joints on

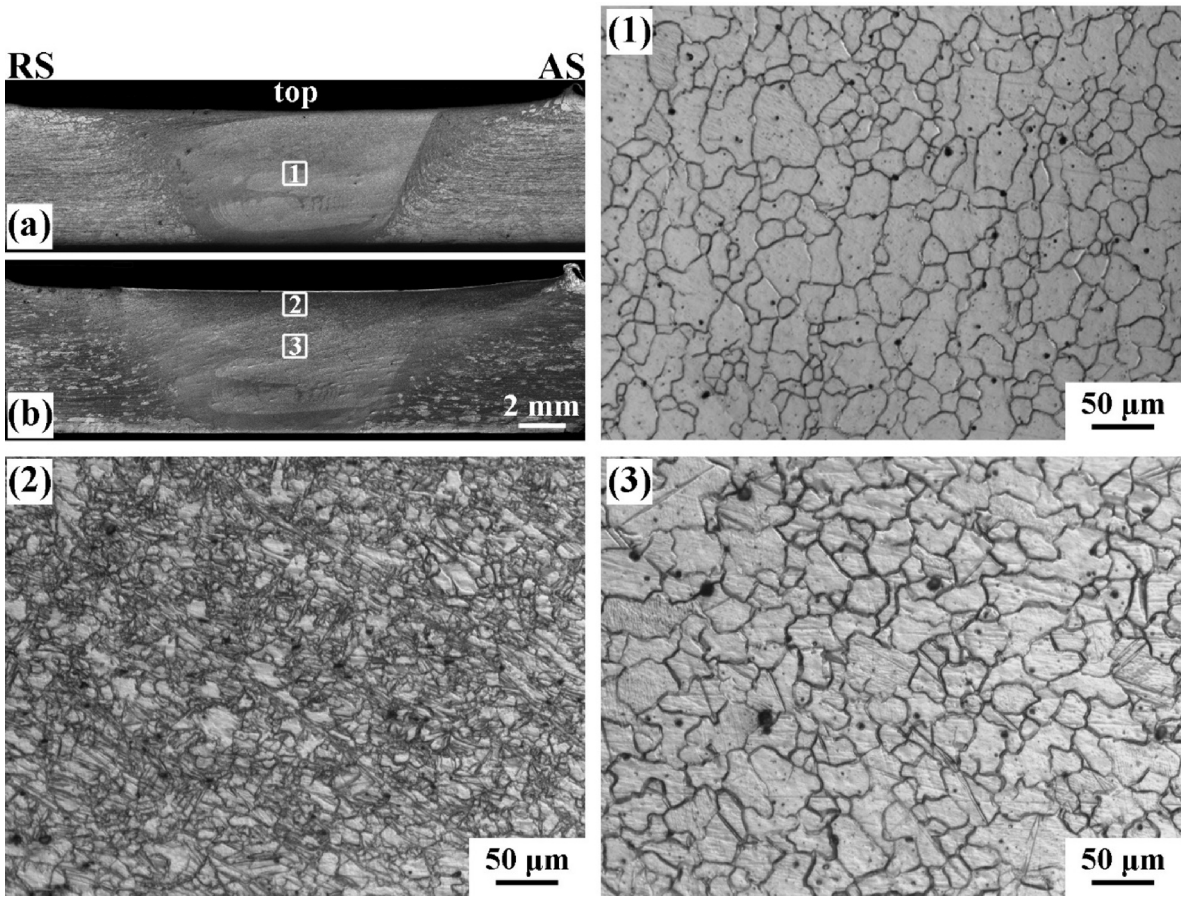

Fig. 2. Cross-sectional overview of (a) original joint and (b) joint subjected to FSP-1, and optical microstructure obtained from regions 1 (1), 2 (2), and 3 (3) in Fig. 2a and b.

the transverse cross-sections by a Vickers hardness tester with a load of 1.96 N and a duration of 10 s.

3. Results and discussion

3.1. Parameter optimization

As indicated in Table 1, many FSP parameters were tested in an attempt to enhance the FSW joint strength through process optimization. The earliest tested parameter combination was denoted as FSP-1, with a rotational rate of 200 rpm, an advancing speed of 50 mm/min, and a nominal penetration depth of 0.4 mm. As shown in Fig. 2a and its relevant sub-figure 1, fully dynamic recrystallized microstructure with no twin structures was attained in the SZ of FSW joint. Although twinning would take place amid the grain structure evolution process during FSW, little of twin structures could be remained at final stage, as reported by Suhuddin et al. (2009). This is ascribed to the high heat input, high strain rate imposed by the FSW tool under typical parameters (e.g. FSW parameters adopted in this work) and the intrinsic preference of Mg alloy for recrystallization. After implementation of additional FSP-1 comparatively low heat input and strain rate, appreciable numbers of deformation twin lamellae were successfully introduced into the upper part of the SZ (Fig. 2b). The depth of the twinned area beneath the tool is about 2 mm; the amount of twinning decreases gradually with the location moving downwards from the top, as illustrated in sub-figure 2 and 3 in Fig. 2. It is suggested that the formation of twins is closely concerned with the squeezing force imposed by the pinless rotational tool.

As shown in Fig. 1, the inclination and periodical movement of tool implies a complex interaction between the tool and the materials in the original joint, endowing different regions in the SZ different loading histories. This character makes the technique obviously different from processing methods like post-rolling, post-tension, and post-compression, in which the loading strain is uniaxial and invariable within the processing area. In a simplified view, the materials were mainly subjected to a vertical compression during FSP.

As reported by Xin et al. (2012) that abundant extension twin boundaries can exert a strengthening and toughening effect by grain subdivision and texture modification, expansion of the twinned area to the whole SZ could be effective to enhance the joint performance. In order to achieve a greater squeezing effect, the processing parameters of FSP-2 and FSP-3 (Table 1) with increased penetration depth were then applied. As shown in Fig. 3a and its relevant sub-figure 1, the twinned area in the SZ was not expanded after FSP-2 in comparison with the effect of FSP-1. In addition to the twin structures, fine recrystallized grains were found to form along the original grain boundaries (sub-figure 1 in Fig. 3). After application of FSP-3 with greater nominal plunge depth value than FSP-2, the upper part of SZ got fully recrystallized and no twins were remained (sub-figure 2 in Fig. 3). The disappearance of twin structures can be attributed to the excessive heat generation caused by the more intense tool/workpiece interaction. This more severe thermo-mechanical coupling effect led to complete dynamic recrystallization instead of twinning. It is quite hard to enlarge the twinned area by just increasing the plunge depth.

In the FSP process, as in FSW, the heat generation is from the friction at the tool/material interface and the plastic deformation of the material. The material stir effect is obviously reduced by using the pinless tool, and thus the heat generated during FSP is estimated to be mainly from the friction between the tool and material. Similar to the heat generation analysis by Schmidt et al. (2004), a simplified equation

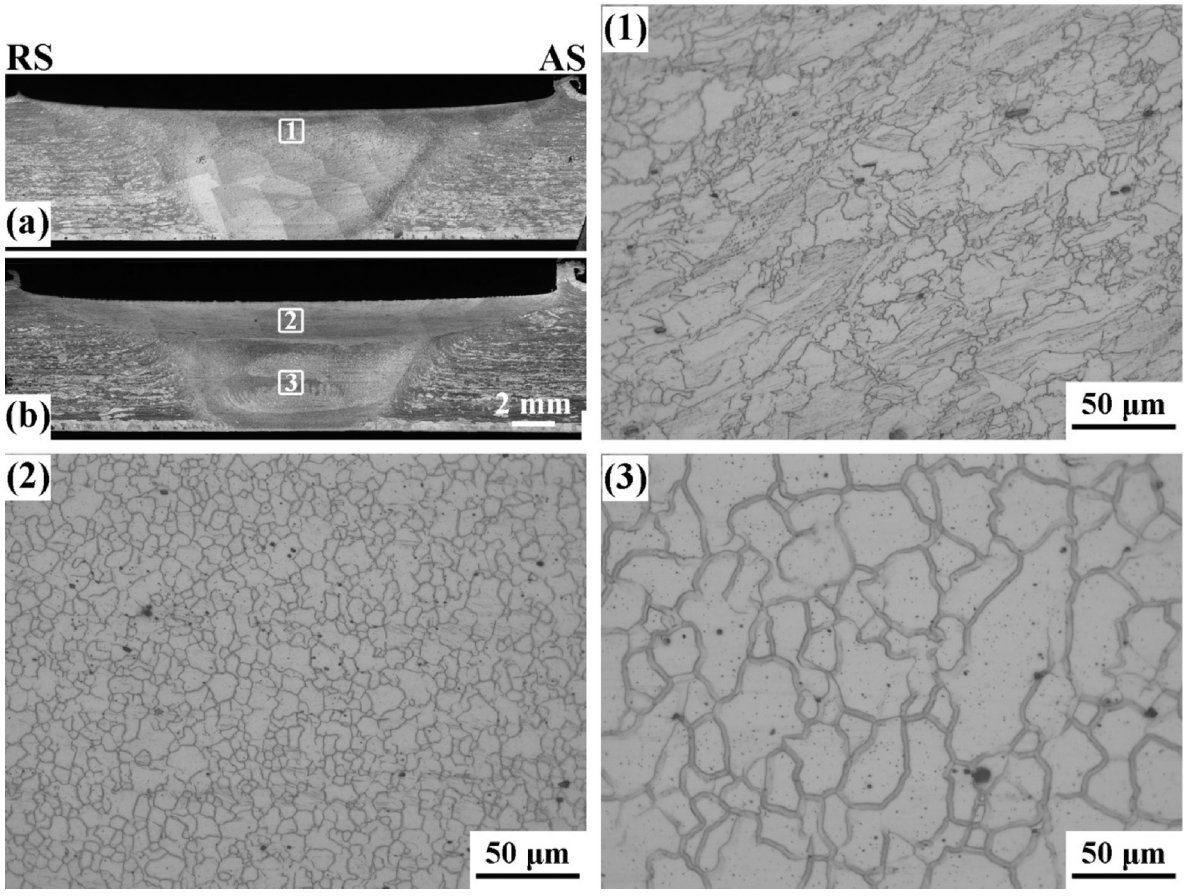

Fig. 3. Cross-sectional overview of joints (a) subjected to FSP-2 and (b) subjected to FSP-3, and optical microstructure obtained from regions 1 (1), 2 (2), and 3 (3) in Fig. 3a and b.

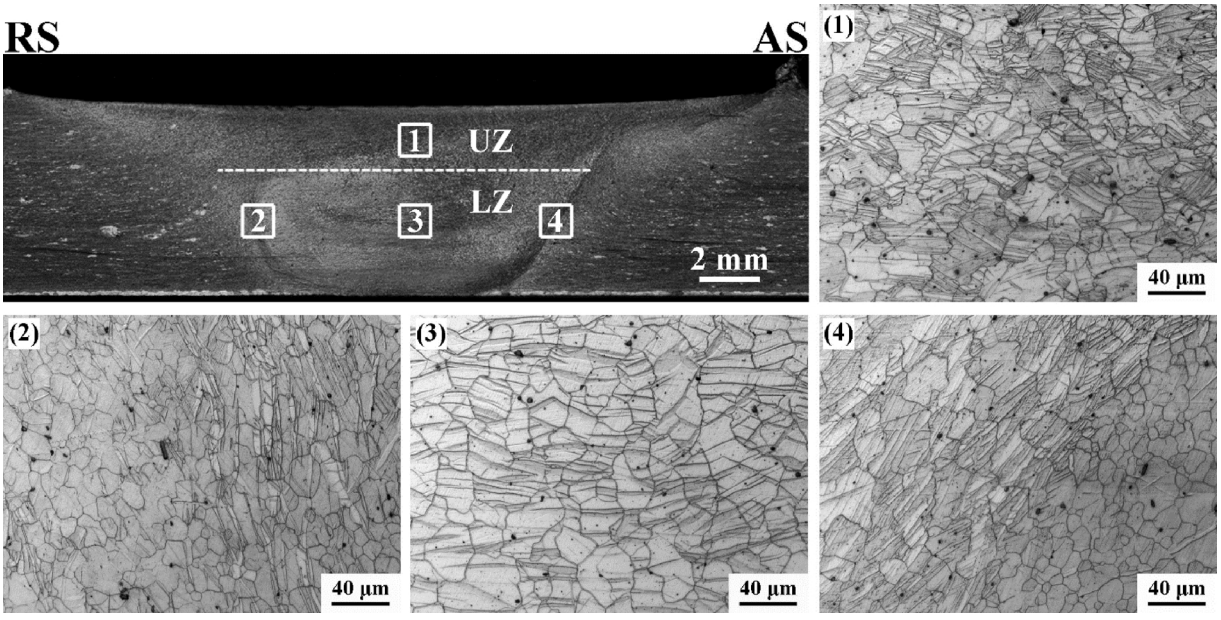

Fig. 4. Cross-sectional overview of joint subjected to FSP-5 and optical microstructure obtained from regions 1 (1), 2 (2), 3 (3), and 4 (4) in the joint.

was derived to describe the rate of heat generation Q under the tool shoulder in this FSP method, which is given as

$$Q = \frac{2}{3}\pi\omega R_{tool}^{3}\left[\eta\mu p + (1-\eta)\frac{\sigma_{yield}}{\sqrt{3}}\right], \quad (1)$$

where ω is the tool rotation rate, R_{tool} is the shoulder radius of the FSP tool, μ is the friction coefficient, p is the contact pressure, σ_{yield} is the material yield stress, and η ($0 \le \eta \le 1$) is a variable to describe the contact condition of the tool/workpiece interface, corresponding to sticking when $\eta = 0$, sliding when $\eta = 1$, partial sliding/sticking when

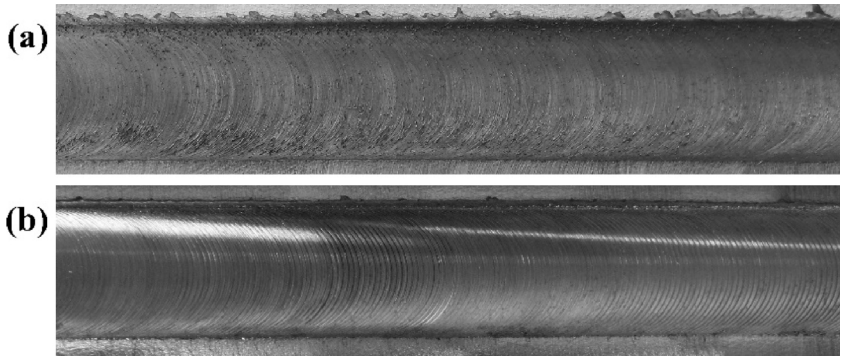

Fig. 5. Surface appearance of (a) original weld and (b) weld subjected to FSP-5.

Table 2
Transverse tensile properties of base material (BM) and joints.

	YS, MPa	TS, MPa	El, %	Joint efficiency, %
BM	158 ± 5	243 ± 3	12.8 ± 0.9	
FSW	96 ± 6	224 ± 0	7.3 ± 1.1	91.1
FSP-1	99	233	8.0	94.7
FSP-2	98	222	5.4	90.2
FSP-3	97	209	5.2	85.0
FSP-4	120	236	6.8	96.0
FSP-5	122 ± 6	246 ± 2	7.8 ± 0.3	100.0

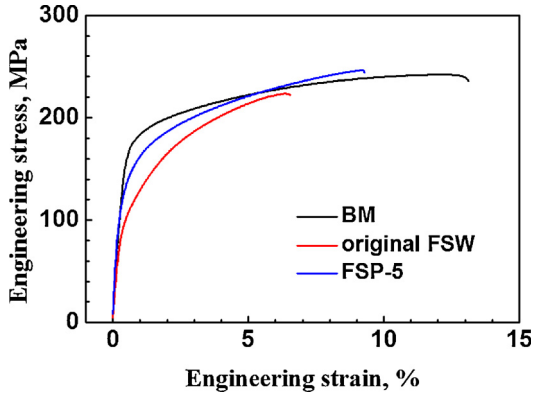

Fig. 6. Tensile engineering stress vs. engineering strain curves of original joint and joints subjected to FSP-5.

$0 < \eta < 1$. The equation indicates that a higher heat generation rate can be obtained with the increase of tool rotation rate ω and contact pressure p, which is positively related to the nominal penetration δ. As for the effect of another critical FSP variable, advancing speed ν, the study by Arbegast and Hartley (1998) suggests that the peak temperature would decrease with increased ν.

The processing parameters of FSP-4 and FSP-5 (Table 1) with lower rotational rate were then adopted in order to reduce the heat input while maintaining a large squeezing force. The whole SZs of the FSP-4 and FSP-5 samples were successfully filled with deformation twins, as shown in Fig. 4.

Fig. 5 exhibits the surface formation of the original FSW weld and the processed weld under FSP-5. It is noted that the additional FSP-5 improved the weld visually. The surface of the FSW weld gets smoother and cleaner after additional FSP-5. This can be attributed to the inactive surface oxidation due to the low heat generation during the additional FSP-5. The lowest heat generation in FSP-5 gave rise to the best visual result of all welds processed by additional FSP.

3.2. Tensile properties and microhardness distribution

The transverse tensile properties of the FSW joints that were subjected to additional FSP passes with different parameters (Table 1) are summarized in Table 2. All the processed joints with FSP parameters that can introduce twin lamellae (i.e., FSP-1, FSP-4, FSP-5) showed enhanced yield strength (YS) and tensile strength (TS) compared to the original FSW joints, which confirms the positive effect of twinning behavior. Under the processing parameters of FSP-5, the tensile properties of the joint were significantly improved; the YS was enhanced to 122 MPa and the TS to 246 MPa, achieving an excellent joint efficiency (the ratio of TS between joint and BM) of 100%. The associated engineering stress–strain curves are given in Fig. 6. It is proved possible to enhance the joint performance by additional FSP under appropriate process variables.

As shown in Fig. 4, the SZ of the joint processed under the parameters of FSP-5 is of a two-layered structure, i.e., the upper zone (denoted as UZ) beneath the shoulder and the lower zone (denoted as LZ) in an elliptical shape. This microstructure-based region division can be simply ascribed to the diminishing tool-imposed load stress with increasing material thickness. The micro hardness distribution was measured in lines along the mid-thickness of the UZ and LZ of the processed joints, and at the same locations on the original joints, as presented in Fig. 7. The micro hardness values in both the UZ and LZ were enhanced

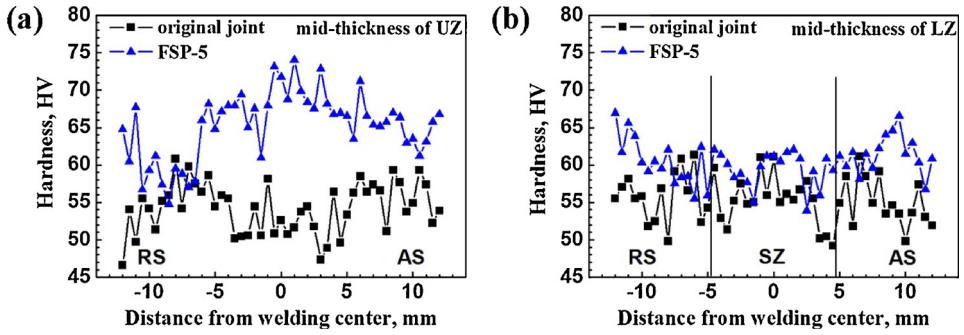

Fig. 7. Cross-sectional hardness profiles of original joint and joint subjected to FSP-5 along mid-thickness of (a) UZ and (b) LZ.

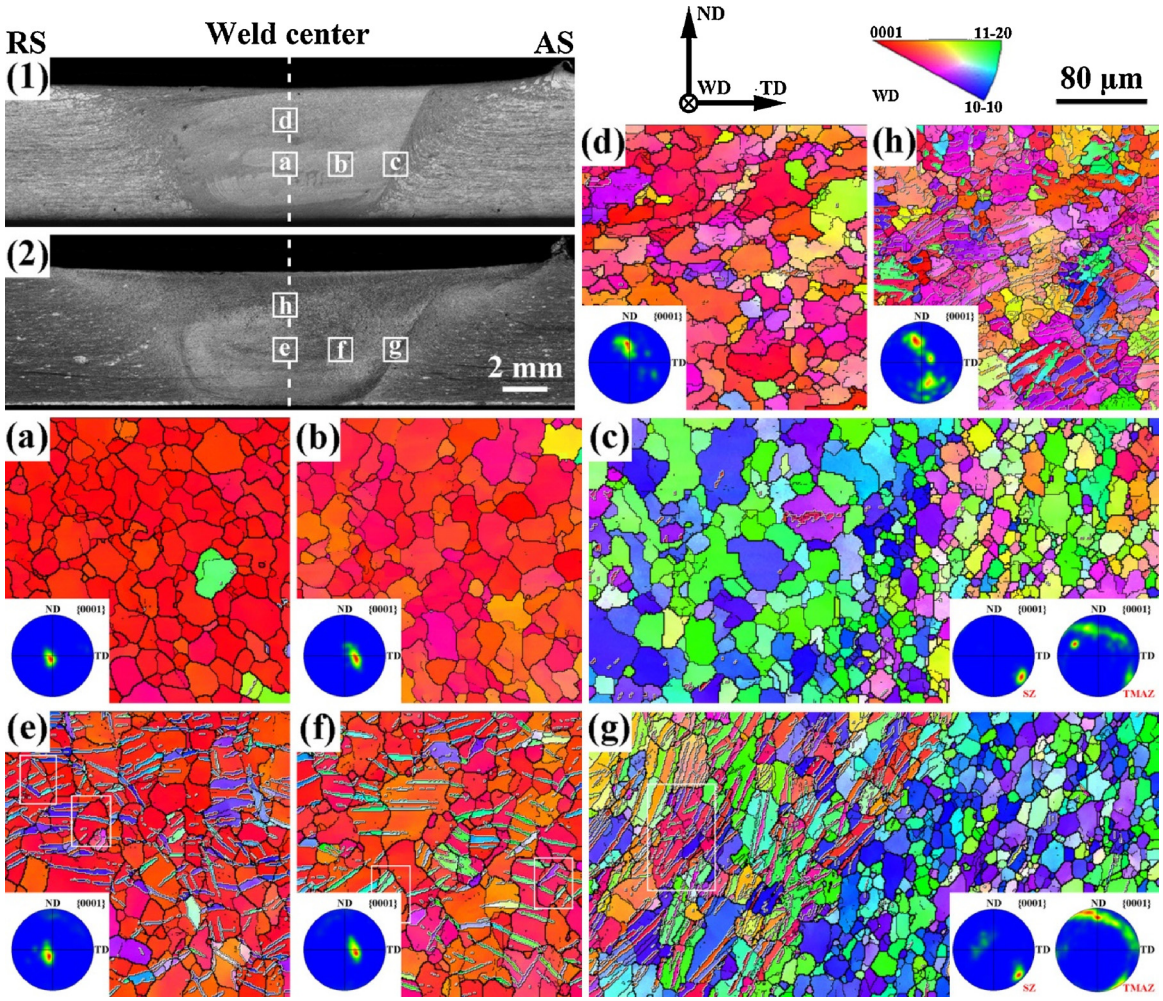

Fig. 8. Cross-sectional overview of (1) original joint and (2) joint subjected to FSP-5, and EBSD orientation maps and pole figures characterized from regions a (a), b (b), c (c), and d (d) in sub-figure (1), and from regions e (e), f (f), g (g), and h (h) in sub-figure (2).

after the additional FSP-5. The hardening effect of FSP-5 in the UZ was more pronounced that in the LZ.

The enhancement of the tensile properties and the hardness values can be rationalized by the strengthening effect of the subsequent deformation. Ascribed to the strong texture formed in the SZ, the grain boundaries with low misorientation can provide limited obstacle effect for motion of dislocations and transmission of twins, giving rise to relatively low k values (Hall-Petch slopes) in FSW Mg alloys compared with those of Mg alloys prepared by other processing methods (Yu et al., 2018). The grain refinement effect for hardness enhancement was not that prominent compared with the twinning-induced hardening effect. Despite the verified positive contribution of twin lamellae, the structure–property relationship in FSPed joints is not entirely clarified. The increase in hardness and the specific hardness distribution necessitate a detailed characterization of the microstructure and texture variation in different sub-regions of the joint. The origin of the improved tensile properties is more complicated, as the microstructure and mechanical properties varied in different sub-regions. Strain localization, as a result of this inhomogeneity, was confirmed by Liu et al. (2014) and Shang et al. (2017b) to be the main factor in determining the premature failure and thus the overall performance of the joint. Therefore, a comparative study of the actual strain distribution in tensile tests is required to analyze the enhancement of mechanical properties. These issues are discussed in detail in the following sections.

3.3. Microtexture evolution after additional FSP

The comparative EBSD measurements of the microtexture evolution in the SZ before and after additional FSP-5 are illustrated in Fig. 8. The orientation color maps were plotted by inverse pole figure (IPF) color-coding, using the WD as reference direction. For the original joints, a special microtexture distribution can be observed in the SZ, i.e., the poles of the c-axes gradually deviate from the WD in a rotation around the ND with the location moving away from the SZ center to the boundary between the SZ and the thermo-mechanically affected zone (TMAZ).

This typical texture distribution has been widely reported in many previous publications on FSW/FSP Mg alloys. It was also suggested by Shang et al. (2017a) that the microtexture near the SZ/TMAZ boundary is different between the AS and RS, i.e., the normal directions of the basal planes on the RS are adjacent to the TD, while that on the AS are usually inclined to the ND from the TD. The pole figures in Fig. 8c revealed that the (0001) basal planes near the SZ/TMAZ boundary on the AS are arranged approximately along the boundary line, which deviates from the ND at an angle of about 40°.

For the processed joint subjected to FSP-5, the orientation maps (Fig. 8e–h) confirmed the substantial multiplication of $\{10\bar{1}2\} < 10\bar{1}1 >$ extension twins (identified by the $86° < 11\ \bar{2}\ 0 > \pm 5°$ misorientation across the twin boundary) in both the UZ and LZ. It was noted that twinning transmission over grain boundaries acted as a major deformation mechanism in additional FSP, especially in the

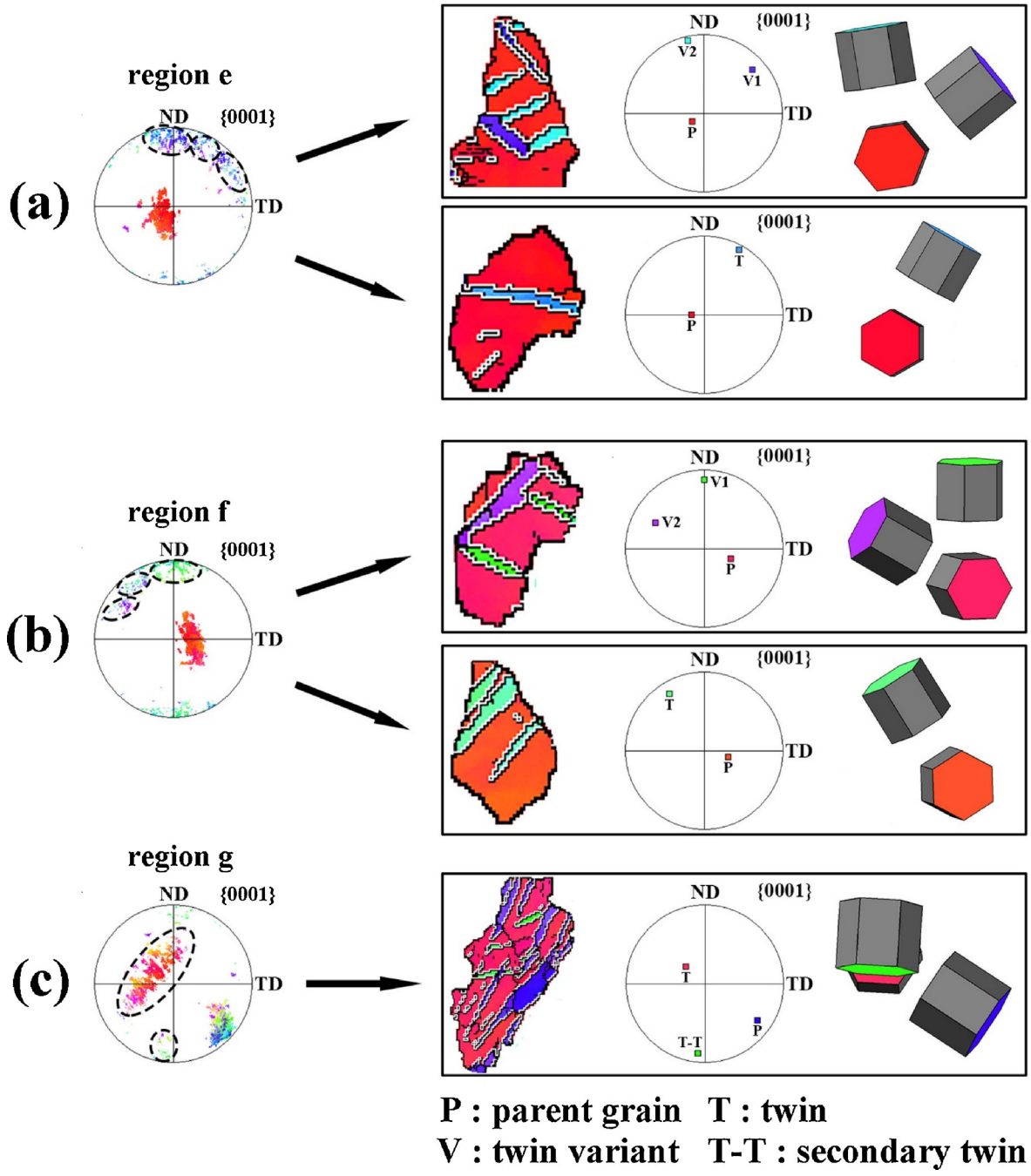

Fig. 9. Analysis on orientation components and twin variant selection at region e (a), region f (b) and region g (c) in the LZ.

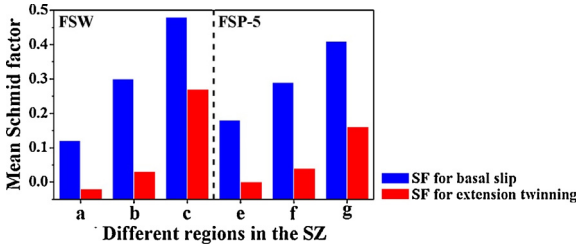

Fig. 10. Mean Schmid factors (SFs) for basal slip and extension twinning at different sub-regions of SZ before and after additional FSP-5.

LZ. Xin et al. (2014b) also found similar twin band structures in the rolling of FSW AZ31, and ascribed the phenomenon to the high value of the geometrical compatibility factor m' between neighboring twins across grain boundaries. Hong et al. (2016) and Huang and Xin (2017) analyzed the correlation between m' and grain boundary misorientation, and confirmed the more frequent twin transmission with decreasing misorientation angle. The strong basal texture that evolved in the LZ endowed the neighboring grains with ideal misorientations below 30°, giving rise to the preferred activation of such twin structures.

The pole figures (Fig. 8) indicate the introduction of new texture components in various regions of the LZ, derived from the lattice reorientation within twins. Although there are six possible twin variants in the activation of extension twins, the convergence of new twin orientations at certain positions in the pole figures revealed a preference

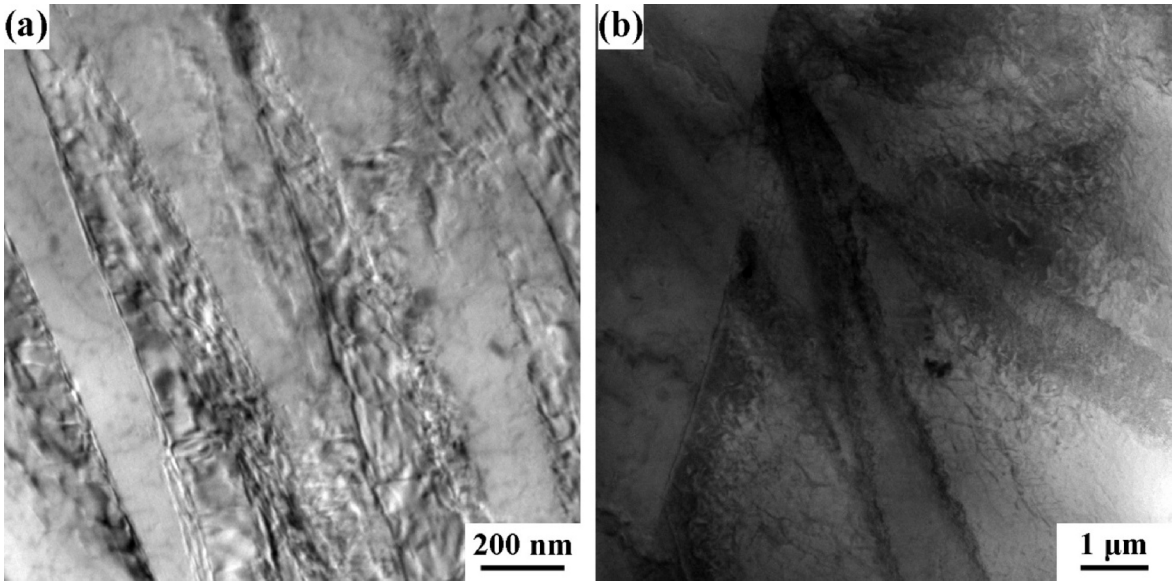

Fig. 11. TEM characterization at (a) UZ and (b) LZ of the joint subjected to FSP-5, showing the different sizes of twin structures.

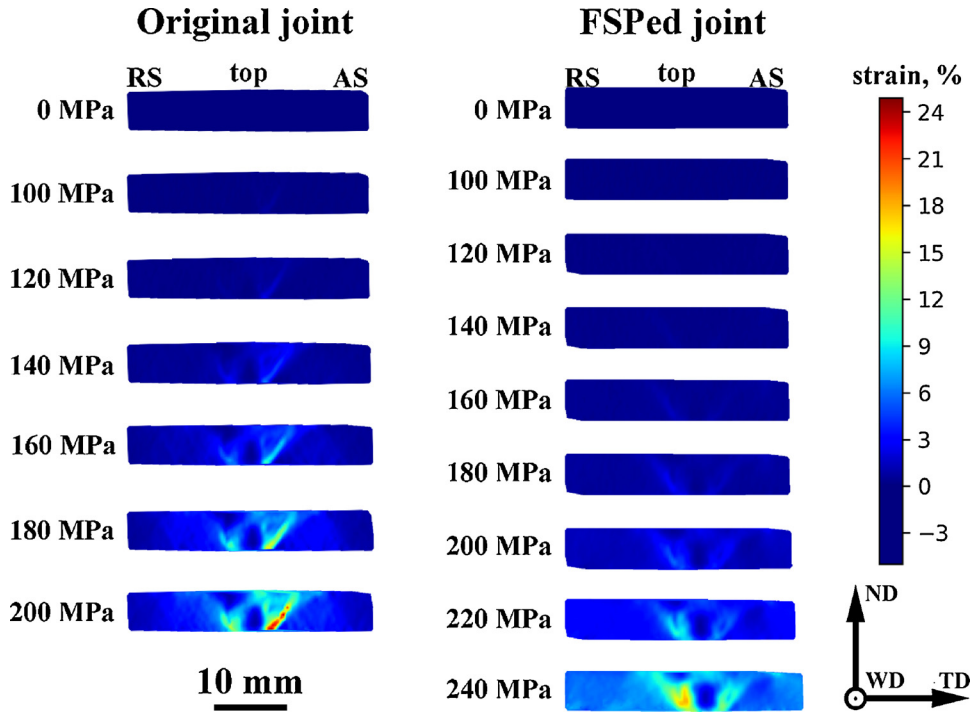

Fig. 12. Distribution of local tensile strains on the same sides of original joint and joint subjected to FSP-5 at different stress levels.

in the selection of certain variants. By verifying the variants selected, the loading state applied in various regions during the additional FSP can be better understood via converse illation, according to the report by Hong et al. (2010, 2011) that the variant selection is significantly dependent on the strain path.

In region (e) (in the center of the LZ with slight position deviation to the RS), the basal poles of twins were concentrated close to the ND with appreciable scatter to the TD on the AS, as illustrated in Fig. 9a. Further analysis revealed that these new orientations stemmed from different twinning behaviors. It is noted that in some grains, two twin variants were simultaneously selected, suggesting a similar propensity for activation. As theoretically analyzed by Hong et al. (2010) based on the Schmid law, uniaxial compressive strain perpendicular to the c-axis would give rise to $\{10\bar{1}2\}$ twinned regions with c-axes placed within ± 30° deviation from the load direction. When the loading axis is parallel to the a-axis, two twin variant pairs have the highest Schmid factor (SF) value of 0.374. When the loading axis is perpendicular to the $\{10\bar{1}0\}$ planes, only one twin variant pair has the highest SF value of 0.499. From the variant selection behavior in region (e), it can be deduced that the local loading stress was not just vertically downward (ND). The compressive stress direction should be aligned at a deflection of about 30°from ND to TD, implying that a horizontal stress component, directed from the LZ center to the LZ side on the RS also existed.

In region (f) (located in the middle place between LZ center and LZ side on the AS), the c-axes of twins also converged in different places. The relative twinning behaviors were analyzed and are illustrated in Fig. 9b. From the characteristics of the twin variants selection, it was revealed that the load in region (f) was comprised of two parts. One

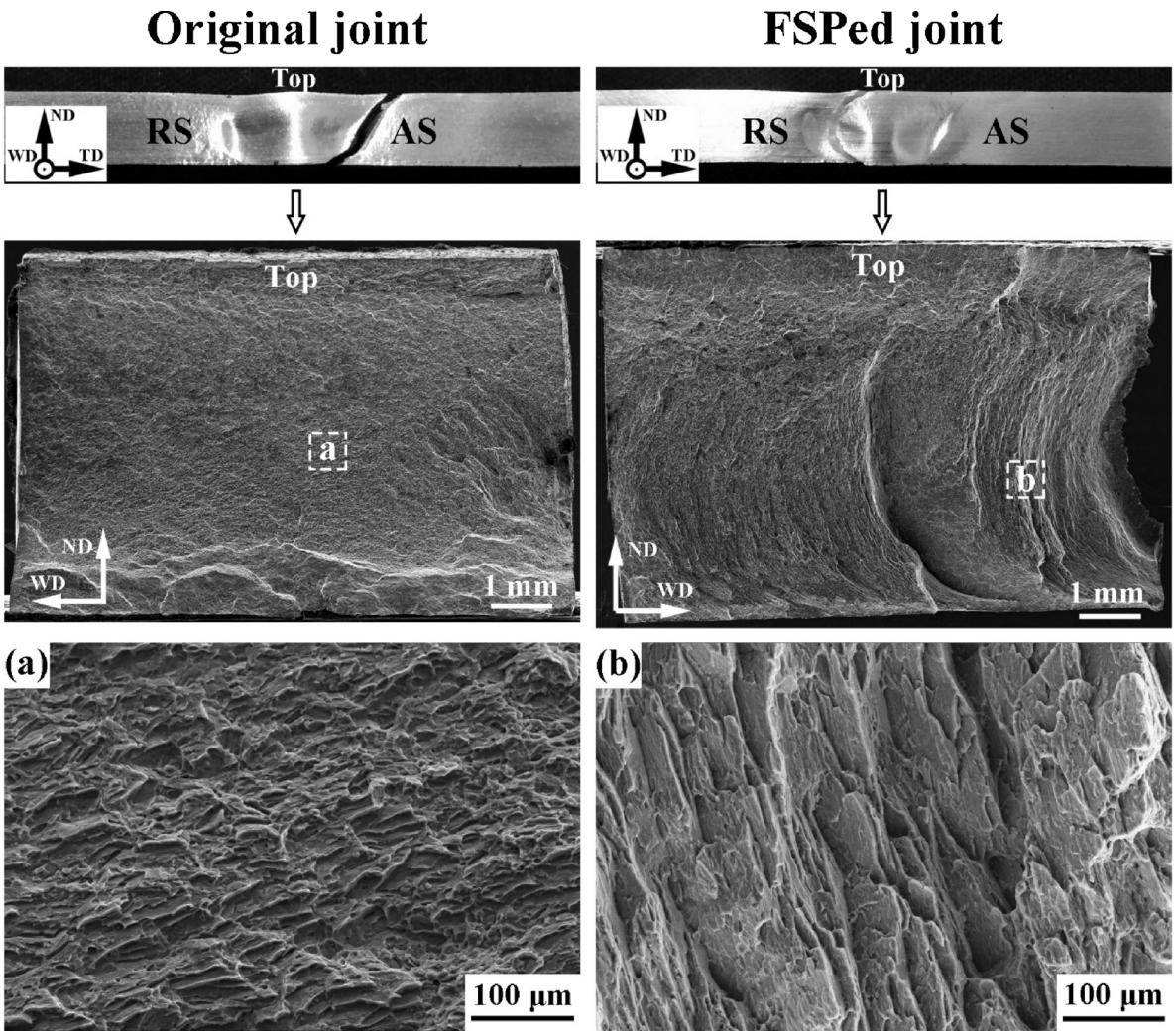

Fig. 13. Fracture locations and macroscopic fractographs of original joint and joint subjected to FSP-5, and microscopic fractographs obtained from regions a (a) and b (b).

load component was vertically downward and the other was directed from the LZ center to the LZ side on the AS. In region (g) (at the edge of the LZ, on the AS), the main twinning-imposed orientations concentrated in one place obviously deviated from the ND, which is very different from the twinning characteristics in regions (e) and (f). This might be ascribed to the remarkable deviation of c-axes in the original grains from the WD–TD plane, and the more complicated local load state, allowing for the orientation analysis depicted in Fig. 9c. The selection of the secondary extension twin variant also suggested the existence of compressive strain in the ND. The analysis about the load state of different sub-regions in the LZ suggested that the applied loading stress to the whole LZ during the additional FSP was specifically directed in the ND–TD plane.

It is generally accepted that the basal slip and $\{10\bar{1}2\} < 10\bar{1}1 >$ extension twinning are predominantly operative in the deformation of AZ31 at room temperature, as their critical resolved shear stresses (CRSS) are much lower than that of non-basal slips and other twinning systems. Clarification of the FSP-induced variation in activating the two dominant deformation modes in tensile tests can thus help to rationalize the improvement of joint performance after FSP. The mean SF for basal slip and $\{10\bar{1}2\}$ twinning were calculated based on grain orientations in different sub-regions of the LZ, as shown in Fig. 10. In the calculation, all possible basal slip systems and $\{10\bar{1}2\}$ twin variants were considered, but only those with the largest SF are presented.

In the original joint, the mean SF for basal slip and $\{10\bar{1}2\}$ twinning varies from place to place. In region (a), the mean SF for basal slip (0.12) and that for $\{10\bar{1}2\}$ twinning (-0.02) are quite small, indicating the difficulty for them to initiate in the center of the SZ. In region (b), the mean SF for basal slip (0.30) is considerably greater than that for $\{10\bar{1}2\}$ twinning (0.03). This illustrates that basal slip is easy to activate in that area. In region (c), a favorable mean SF can be found for basal slip (0.48) as well as extension twinning (0.27), implying that both deformation modes would be quite active. The different activity of basal slip and $\{10\bar{1}2\}$ twinning in different sub-regions would lead to severe strain localization during tensile deformation. The area near the SZ boundary on the AS would serve as a favorable place for both basal slip and extension twinning. This texture-induced deformation-concentrated region would be susceptible to premature crack initiation, and thus deteriorate the joint strength and ductility. The reinforcement of this region can help to enhance the overall performance of joints.

After the additional FSP, there was little change in the mean SF for basal slip and $\{10\bar{1}2\}$ twinning in region (f) compared to region (b). In region (g), however, the mean SF value decreased from 0.48 to 0.41 for basal slip, and the mean SF for extension twinning decreased from 0.27 to 0.16 compared to region (c). In region (e), the mean SF for both basal slip and $\{10\bar{1}2\}$ twinning slightly increased compared to region (a). Although the change of mean SF value was small, the discrepancy of deformation capability in different regions was visibly reduced. Equivalent grain refinement hardening was also achieved due to the grain subdivision by substantial twin lamellae. It is proved that the

additional FSP could be effective to strengthen the region near the SZ boundary on the AS and relieve the deformation concentration behavior.

Despite the new twinning-imposed texture, the matrix grain orientations in various regions of the LZ showed little change in comparison with the original joint, whereas the texture evolution in the UZ was much more complicated. As seen in the orientation maps (Fig. 8), the volume fraction of deformation twins in the UZ is obviously larger than that in the LZ after the additional FSP, implying that the UZ experienced more severe plastic deformation than the LZ.

In the UZ of joint, the texture evolution (Fig. 8d–h) showed that the c-axes of grains evolved to be roughly parallel to the ND, which hinders involvement of both basal slip and $\{10\bar{1}2\}$ twinning in transverse tensile tests, contributing to the enhancement of yield strength. The TEM observations (Fig. 11) showed that the size of some twins in the UZ were much smaller than those in the LZ. As the twin boundaries can effectively hinder the movement of dislocations, like grain boundaries, a better strengthening effect was achieved in the UZ due to the more severe grain refinement from the extensive twin boundaries. For these reasons, the increase of hardness in the UZ is significantly larger than that in the LZ after the additional FSP.

3.4. Strain distribution evolution and fracture

As the strain localization is the main factor deteriorating the joint performance, it is necessary to verify the actual strain distribution that evolves during tensile tests. The DIC measurement (Fig. 12) illustrates the distribution of tensile strains at different tensile stress levels, of the original and FSPed joints. The strain localization differed between the two joints. In the original joint, the tensile strain gradually concentrated in a narrow area along the SZ-boundary on the AS, agreeing well with the local high mean SF values for both basal slip and $\{10\bar{1}2\}$ twinning. After the additional FSP, the strain localization was significantly weakened at the same stress levels, and the strain concentration area in the SZ shifted from the AS to the RS.

As shown in Fig. 13, the fracture locations of the two joints were in accordance with the strain localization characteristics; the fracture of the original joint coincided with the SZ edge on the AS, while the fracture of the FSPed joint passed through the area located approximately in the middle of the SZ center and SZ edge on the RS. The SEM fractographs showed that the fracture surface of the original joint was relatively flat, while the fracture morphology of the failed FSPed joint was far more rough and complicated, indicating twists and turns in crack propagation. The complex character of crack growth in the FSPed joint appeared to be associated with the “onion ring” structure (i.e., stacking shear layers) formed in the SZ, confirmed by Mironov et al. (2017) and Shang et al. (2017a).

In general, the subsequent FSP process can not only weaken the strain localization but also change the fracture behavior. Reinforcement of the weaker regions, that are susceptible to crack initiation, can thus postpone the premature failure that usually occurs in FSW Mg alloys.

4. Conclusions

(1) The additional FSP technique was proved feasible and effective to enhance the joint performance of original FSW joint via optimization of processing parameters. By reducing the heat generation and increasing the applied loading stress in FSP, abundant twin lamellae were successfully introduced to the whole SZ.
(2) The strengthening effect of additional FSP stemmed from the twinning-induced microstructure refinement and the weakened strain localization resulted from the twinning-induced texture modification, which were proved by the SF analysis and DIC observation.
(3) Compared with other methods for joint improvement, the FSP technique exhibits unique advantages in practical use for welding automation and welding intelligence due to its flexibility and limited processing scale. The FSP technique also shows great potential in optimization of welds on workpieces with complicated geometry like curved surfaces, hollow extrusion and so on.

Acknowledgment

This work was supported by the National Natural Science Foundation of China under Grant Nos. 51331008, U1760201, and 51371179.

References

Arbegast, W.J., Hartley, P.J., 1998. Pine Mountain, GA, USA, JuneProceedings of the Fifth International Conference on Trends in Welding Research1998. Proceedings of the Fifth International Conference on Trends in Welding Research 1–5.
Commin, L., Dumont, M., Masse, J.-E., Barrallier, L., 2009. Friction stir welding of AZ31 magnesium alloy rolled sheets: influence of processing parameters. Acta Mater. 57, 326–334.
Hong, S.-G., Park, S.H., Lee, C.S., 2010. Role of {10–12} twinning characteristics in the deformation behavior of a polycrystalline magnesium alloy. Acta Mater. 58, 5873–5885.
Hong, S.-G., Park, S.H., Lee, C.S., 2011. Strain path dependence of {10–12} twinning activity in a polycrystalline magnesium alloy. Scr. Mater. 64, 145–148.
Hong, X., Godfrey, A., Liu, W., 2016. Challenges in the prediction of twin transmission at grain boundaries in a magnesium alloy. Scr. Mater. 123, 77–80.
Huang, Q.L., Xin, R.L., 2017. Correlation between boundary misorientaion and a geometric parameter for cross-boundary twins in Mg alloys. Adv. Eng. Mater. 19 (3), 1600614.
Lee, C.J., Huang, J.C., Du, X.H., 2007. Improvement of yield stress of friction-stirred Mg-Al-Zn alloys by subsequent compression. Scr. Mater. 56, 875–878.
Liu, D.J., Xin, R.L., Xiao, Y., Zhou, Z., Liu, Q., 2014. Strain localization in friction stir welded magnesium alloy during tension and compression deformation. Mater. Sci. Eng. A 609, 88–91.
Liu, Z., Xin, R.L., Li, D.R., Sun, L.Y., Liu, Q., 2016. Comparative study on twinning characteristics during two post-weld compression paths and their effects on joint enhancement. Sci. Rep. 6, 39779.
Mironov, S., Onuma, T., Sato, Y.S., Yoneyama, S., Kokawa, H., 2017. Tensile behavior of friction-stir welded AZ31 magnesium alloy. Mater. Sci. Eng. A 679, 272–281.
Mishra, R.S., Ma, Z.Y., 2005. Friction stir welding and processing. Mater. Sci. Eng. R Rep. 50, 1–78.
Padhy, G.K., Wu, C.S., Gao, S., 2018. Friction stir based welding and processing technologies-processes, parameters, microstructures and applications: a review. J. Mater. Sci. Technol. 34, 1–38.
Park, S.H.C., Sato, Y.S., Kokawa, H., 2003a. Basal plane texture and flow pattern in friction stir weld of a magnesium alloy. Metall. Mater. Trans. A 34, 987–994.
Park, S.H.C., Sato, Y.S., Kokawa, H., 2003b. Effect of micro-texture on fracture location in friction stir weld of Mg alloy AZ61 during tensile test. Scr. Mater. 49, 161–166.
Raja, A., Pancholi, V., 2017. Eff ;ect of friction stir processing on tensile and fracture behaviour of AZ91 alloy. J. Mater. Process. Technol. 248, 8–17.
Schmidt, H., Hattel, J., Wert, J., 2004. An analytical model for the heat generation in friction stir welding. Model. Simul. Mater. Sci. Eng. 12, 143–157.
Shang, Q., Ni, D.R., Xue, P., Xiao, B.L., Ma, Z.Y., 2017a. Evolution of local texture and its effect on mechanical properties and fracture bahavior of friction stir welded joint of extruded Mg-3Al-1Zn alloy. Mater. Charact. 128, 14–22.
Shang, Q., Ni, D.R., Xue, P., Xiao, B.L., Ma, Z.Y., 2017b. Improving joint performance of friction stir welded wrought Mg alloy by controlling non-uniform deformation behavior. Mater. Sci. Eng. A 707, 426–434.
Suhuddin, U.F.H.R., Mironov, S., Sato, Y.S., Kokawa, H., Lee, C.-W., 2009. Grain structure evolution during friction-stir welding of AZ31 magnesium alloy. Acta Mater. 57, 5406–5418.
Woo, W., Choo, H., Brown, D.W., Liaw, P.K., Feng, Z., 2006. Texture variation and its influence on the tensile behavior of a friction-stir processed magnesium alloy. Scr. Mater. 54, 1859–1864.
Xie, G.M., Ma, Z.Y., Geng, L., 2008. Effect of microstructural evolution on mechanical properties of friction stir welded ZK60 alloy. Mater. Sci. Eng. A 486, 49–55.
Xin, Y.C., Wang, M.Y., Zeng, Z., Nie, M.G., Liu, Q., 2012. Strengthening and toughening of magnesium alloy by {10–12} extension twins. Scr. Mater. 66, 25–28.
Xin, R.L., Liu, D.J., Xu, Z.R., Li, B., Liu, Q., 2013. Changes in texture and microstructure of friction stir welded Mg alloy during post-rolling and their effects on mechanical properties. Mater. Sci. Eng. A 582, 178–187.
Xin, R.L., Sun, L.Y., Liu, D.J., Zhou, Z., Liu, Q., 2014a. Effect of subsequent tension and annealing on microstructure evolution and strength enhancement of friction stir welded Mg alloys. Mater. Sci. Eng. A 602, 1–10.
Xin, R.L., Guo, C.F., Xu, Z.R., Liu, G.D., Huang, X.X., Liu, Q., 2014b. Characteristics of long {10–12} twin bands in sheet rolling of a magnesium alloy. Scr. Mater. 74, 96–99.
Yang, J., Ni, D.R., Wang, D., Xiao, B.L., Ma, Z.Y., 2014. Friction stir welding of as-extruded Mg-Al-Zn alloy with higher Al content. Part I: formation of banded and line structures. Mater. Charact. 96, 142–150.
Yu, H.H., Xin, Y.C., Wang, M.Y., Liu, Q., 2018. Hall-Petch relationship in Mg alloys: a review. J. Mater. Sci. Technol. 34, 248–256.